FULL PAPER

Cancer Therapy

ADVANCED
FUNCTIONAL
MATERIALS

www.afm-journal.de

Renal-Clearable PEGylated Porphyrin Nanoparticles for Image-Guided Photodynamic Cancer Therapy

Liang Cheng,* Dawei Jiang, Anyanee Kamkaew, Hector F. Valdovinos, Hyung-Jun Im, Liangzhu Feng, Christopher G. England, Shreya Goel, Todd E. Barnhart, Zhuang Liu, and Weibo Cai*

Nanomaterials with renal clearance from the body within a reasonable time-scale have shown great promises in the area of nanomedicine recently. However, the integration of theranostic and renal clearance properties into a single ultrasmall nanostructure remains a great challenge. Herein, *meso*-tetra(4-carboxyphenyl)porphyrin (TCPP) structure is utilized as a model, for the first time using noninvasive dynamic positron emission tomography (PET) imaging to investigate the balance of the renal clearance and tumor uptake behaviors of polyethylene glycol (PEG)-modified porphyrin nanoparticles (TCPP-PEG) with various molecular weights. This study finds that TCPP-PEG nanoparticles with larger molecular weight show higher tumor uptake due to the enhanced permeability and retention effect, while the lower ones tend to be better for renal clearance. Based on dynamic PET and fluorescence dual-modal imaging modalities, the TCPP-PEG$_{10K}$ nanoparticles seem to be an excellent choice for the balance of renal clearance and tumor retention. In vitro and in vivo photodynamic therapy confirms an excellent therapeutic efficacy. Therefore, this work presents a simplified approach to fabricate and select biocompatible multifunctional TCPP-PEG-based theranostic agents with renal clearance behavior, which highlights the clinical application potential of TCPP-PEG nanoparticles as theranostic probes for imaging-guided cancer therapy.

1. Introduction

Cancer has overtaken heart disease to become the leading cause of death worldwide.[1] Fortunately, with the continued development of nanomaterials and nanotechnology, new types of effective cancer treatment, such as photothermal therapy (PTT) and photodynamic therapy (PDT), have emerged as powerful cancer

therapy techniques.[2] Various inorganic/organic nanomaterials including carbon-based nanomaterials, gold-based nanomaterials, metallic nanoparticles, transition metal dichalcogenides, organic polymers, and albumin carriers have shown great potential for cancer treatment due to the unique physiochemical properties.[2a,b,3] However, most of these nanoparticles suffer from high uptake by the reticuloendothelial system (RES), resulting in slow and inefficient clearance. According to the U.S. Food and Drug Administration principle, any diagnostic or therapeutic agent should be completely cleared from the body within a reasonable period of time.[4] Considering the unique structure of the glomerular capillary wall, only ultrasmall nanoparticles with hydrodynamic diameters (HDs) less than 5.5 nm can pass through the kidneys and rapidly undergo renal excretion. Previous studies have shown that nanoparticles ranging from 15 to 50 nm are readily sequestered by the RES, while those nanoparticles larger than 50 nm undergo partial hepatobiliary clearance.[5] In general, renal clearance is much faster than hepatobiliary clearance. Both nanoparticle size and surface coating will affect the HDs and the way in which the nanoparticle is cleared from the body,[5a,6] and it is a great challenge to fabricate renal-clearable nanomaterials.

In clinical applications, increased circulation time and exposure of nanomaterials to healthy tissues have strongly correlated

Dr. L. Cheng, Dr. L. Feng, Prof. Z. Liu
Institute of Functional Nano and Soft Materials (FUNSOM)
Collaborative Innovation Center of Suzhou Nano
Science and Technology
Soochow University
Suzhou, Jiangsu 215123, China
E-mail: lcheng2@suda.edu.cn
Dr. L. Cheng, Dr. D. Jiang, Dr. A. Kamkaew, Prof. H.-J. Im,
Prof. W. Cai
Department of Radiology
University of Wisconsin–Madison
Madison, WI 53705, USA
E-mail: wcai@uwhealth.org

Prof. A. Kamkaew
School of Chemistry
Institute of Science
Suranaree University of Technology
Nakhon Ratchasima 30000, Thailand
Dr. H. F. Valdovinos, Dr. C. G. England, Dr. T. E. Barnhart, Prof. W. Cai
Department of Medical Physics
University of Wisconsin-Madison
Madison, WI 53705, USA
Dr. S. Goel, Prof. W. Cai
Materials Science Program
University of Wisconsin–Madison
Madison, WI 53705, USA

**ADVANCED
SCIENCE NEWS**
www.advancedsciencenews.com

**ADVANCED
FUNCTIONAL
MATERIALS**
www.afm-journal.de

with increased toxicities and adverse effects. However, the rapid removal of nanoparticles by renal clearance results in lower tumor accumulation, weaker imaging sensitivity, and poorer therapeutic effects. Therefore, it is difficult to design nanomaterials that satisfy the balance between the imaging and therapeutic desires and the requirement for renal clearance within a reasonable timescale.[4,5,7] Recently, glutathione-coated ultrasmall gold nanoparticles (2.3 ± 0.3 nm) showed rapid renal clearance. However, the ultrasmall gold nanoparticles displayed slow clearance and gradual passive tumor retention after coating with PEG. Liu et al. also developed iron coordination polymer nanodots with renal clearance properties for cancer theranostic applications.[8] Ultrasmall polymer nanodots showed excellent renal clearance and effectively accumulated in the tumor via the enhanced permeability and retention (EPR) effect for magnetic resonance imaging-guided PTT. However, fabricating renal-clearable nanomaterials with desirable multiple functionalities remains a great challenge.

Herein, we investigate the clearance and tumor uptake behavior of nanoparticles using *meso*-tetra(4-carboxyphenyl)-porphyrin (*m*TCPP) fabricated with polyethylene glycol (PEG) as a model. TCPP and their derivatives are widely employed for cancer diagnosis and PDT, as they have shown enhanced affinity to cancer cells. However, the hydrophobic nature of most porphyrins has limited their potential use in clinic. We hypothesize that the addition of PEG to TCPP would enhance the aqueous solubility and increase the molecular volume, resulting in enhanced tumor localization. Thus, different molecular weights of PEG molecule (2, 5, 10, and 30 K) are conjugated to TCPP, and the resulting TCPP-PEG nanoparticles are tested for clearance and tumor uptake behaviors. Moreover, TCPP is a good chelating agent for the isotope $^{64}Cu^{2+}$, a useful positron emission tomography (PET) radionuclide with a 12.7 h half-life, for PET imaging.[9] As a noninvasive analytical technique, we first investigate the dynamic PET imaging of TCPP-PEG nanoparticles with various molecule weights after intravenous (i.v.) injection. It was found that larger sizes of the nanoparticles are better for tumor uptake, while the smaller ones are more amenable to renal clearance. Under the guidance of PET and fluorescence dual-modality imaging, TCPP-PEG$_{10K}$ nanoparticles with a HD size of ≈10 nm would be a good candidate for balancing of clearance and tumor uptake behaviors. In vitro and in vivo PDT is carried out which gave excellent therapeutic efficacy for the selected nanoparticles. Our study presents a simplified approach to fabricate and indicate biocompatible multifunctional TCPP-PEG-based theranostic agents with clearance behavior, which highlights the clinical application potential of TCPP-PEG nanoparticles as theranostic probes for image-guided cancer therapy.

2. Results and Discussion

TCPP porphyrin nanoparticles with various molecular weights of PEG chains were synthesized using a simple amide coupling reaction (**Figure 1**a). Unlike the previous porphyrin-PEG mesh structure,[10] only a single NH$_2$ terminal of PEG polymer was used. Carboxyl groups on TCPP were first activated with 1-ethyl-3-(3-(dimethylamino)-propyl)carbodiimide

(EDC), and then PEG was added into the reaction with a ratio of 2:1 (TCPP:PEG) to ensure only one carboxyl group of TCPP molecule was conjugated with a single polymer chain of PEG. After the reaction, several suitable filters were used to remove excess free TCPP molecules and coupling reagents. Matrix-assisted desorption/ionization time-of-flight (MALDI-TOF) spectra were used to confirm the molecular weight of the various synthesized TCPP-PEG (2, 5, 10, and 30 K) polymers. From the spectra, we found that mostly single PEG polymers were linked to the surface of TCPP molecules to form TCPP-PEG nanoparticles with various molecular weights based on the PEG used for synthesis (Figure S1, Supporting Information). However, when the ratios of TCPP:PEG changed to 1:1 or lower, mixtures of TCPP-PEG polymers were found in the system and were too complicated to purify (Figure S2, Supporting Information). ^{1}H nuclear magnetic resonance (NMR) and Fourier transform infrared (FTIR) spectra also confirmed that various molecular weight of PEG molecules were conjugated on TCPP (Figures S3 and S4, Supporting Information). From the high-performance liquid chromatography spectra, we also found that the retention time was greatly dependent on the molecular weights of the synthesized TCPP-PEG polymers (Figure S5, Supporting Information). Transmission electron microscopy (TEM) images revealed that all these synthesized porphyrin polymers existed in a micelle structure with sizes of 3.6 ± 1.4, 5.4 ± 2.3, 8.8 ± 1.6, and 14.2 ± 2.8 nm for TCPP-PEG$_{2K}$, TCPP-PEG$_{5K}$, TCPP-PEG$_{10K}$, and TCPP-PEG$_{30K}$, respectively (Figure 1b). By increasing the molecular weight of PEG conjugates, the HDs also increased. The final HDs were 4.6 ± 1.4, 7.5 ± 2.2, 10.1 ± 2.8, and 17.3 ± 3.2 nm for TCPP-PEG$_{2K}$, TCPP-PEG$_{5K}$, TCPP-PEG$_{10K}$, and TCPP-PEG$_{30K}$ nanoparticles, respectively, agreed with the above TEM results (Figure 1c). All these TCPP-PEG nanoparticles were highly stable in various physiological solutions without aggregation for 3 months (Figures S6 and S7, Supporting Information). Zeta potential of all TCPP-PEG nanoparticles was slightly negative (Figure S8, Supporting Information), confirming that parts of TCPP-PEG nanoparticles satisfy the size and surface charge threshold requirements for renal clearance. In addition, there was no fluorescence quenching after PEG conjugation (Figure S9, Supporting Information), indicating that our synthesized TCPP-PEG nanoparticles were viable fluorescence imaging agents.

Porphyrins and their derivatives can be readily radiolabeled with copper-64 ($^{64}Cu^{2+}$) for PET imaging, and dynamic PET imaging provides a highly useful tool for studying renal clearance behavior.[11] By simply mixing $^{64}Cu^{2+}$ with TCPP-PEG nanoparticles at 37 °C for 1 h under constant shaking, we found that $^{64}Cu^{2+}$ was immediately chelated by TCPP-PEG nanoparticles with more than 80% labeling yields for all TCPP-PEG nanoparticles (**Figure 2**a–h). Moreover, the ^{64}Cu-labeled TCPP-PEG nanoparticles (^{64}Cu-TCPP-PEG) were also found to be highly stable in serum for 48 h, even in a 1,4,7-triazacyclononane-1,4,7-triacetic acid (NOTA) competitive situation (Figure 2i–l). Such highly efficient and stable intrinsic radiolabeling of nanoparticles would be suitable for in vivo PET imaging. In order to investigate both clearance and tumor uptake behaviors, we used BALB/c mice bearing murine breast cancer 4T1 tumors. Mice were i.v. injected with ≈10 MBq of various ^{64}Cu-TCPP-PEG nanoparticles (2, 5, 10, and 30 K) and imaged by a microPET/microCT Inveon rodent

**ADVANCED
SCIENCE NEWS**
www.advancedsciencenews.com

**ADVANCED
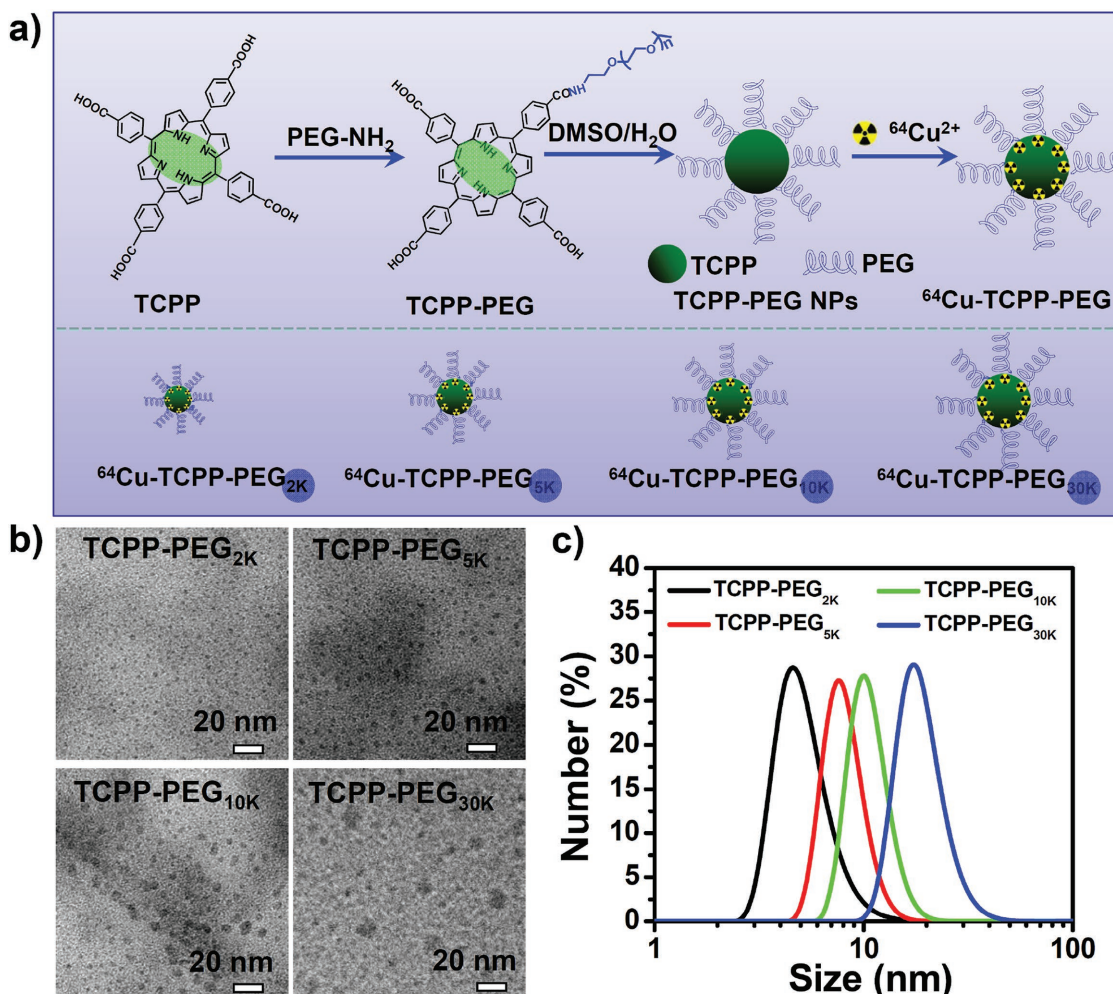FUNCTIONAL
MATERIALS**
www.afm-journal.de

Figure 1. Synthesis and characterization of TCPP-PEG NPs. a) A scheme showing TCPP molecule conjugated with different molecular weight PEG molecules for $^{64}Cu^{2+}$ labeling. b) TEM images of TCPP-PEG$_{2K}$, TCPP-PEG$_{5K}$, TCPP-PEG$_{10K}$, and TCPP-PEG$_{30K}$ nanoparticles. c) The hydrodynamic diameters (HDs) of TCPP-PEG nanoparticles with various molecule weights after being incubated in water solution. The HDs of the particles were 4.6 ± 1.4 nm for TCPP-PEG$_{2K}$, 7.5 ± 2.2 nm for TCPP-PEG$_{5K}$, 10.1 ± 2.8 nm for TCPP-PEG$_{10K}$, and 17.3 ± 3.2 nm for TCPP-PEG$_{30K}$ nanoparticles.

model scanner. **Figure 3**a shows the representative maximum intensity projections of coronal PET images depicting the in vivo biodistribution of ^{64}Cu-TCPP-PEG nanoparticles at 10 s, 1 min, 5 min, 15 min, 30 min, 2 h, 4 h, 6 h, 12 h, and 24 h postinjection (p.i.). During the initial 30 min, a dynamic scan was performed (Figures S10–S13, Supporting Information). Static PET imaging of the same mice was performed to provide more detailed information regarding the clearance of TCPP-PEG nanoparticles at later time points. It was found that all the TCPP-PEG nanoparticles showed high accumulation in the blood pool directly after injection, yet TCPP-PEG nanoparticles were rapidly filtered through kidneys and accrued in the bladder. Interestingly, the blood circulation and metabolic rate showed significant differences among TCPP-PEG nanoparticles with various molecular weights. Figure 3b shows the detailed blood circulation curves of ^{64}Cu-TCPP-PEG nanoparticles during the initial 4 h. Classical two-compartment pharmacokinetics were observed for all the TCPP-PEG nanoparticles (Figure S14a–d, Supporting Information), with distribution half-life ($t_{1/2\alpha}$) and elimination half-life ($t_{1/2\beta}$) values of 4.26 ± 1.95 min and 10.67 ± 2.15 min for

TCPP-PEG$_{2K}$, 10.84 ± 0.35 min and 28.15 ± 3.55 min for TCPP-PEG$_{5K}$, 17.62 ± 3.34 min and 40.05 ± 8.70 min for TCPP-PEG$_{10K}$, 26.83 ± 3.92 min, and 86.9 ± 18.36 min for TCPP-PEG$_{30K}$, respectively. The $t_{1/2\beta}$ of TCPP-PEG$_{30K}$ nanoparticles was 8.1 times longer than that of TCPP-PEG$_{2K}$ nanoparticles. In addition, the area under the curve for TCPP-PEG$_{30K}$ (1082.3%ID h g^{-1}) was 2.6 times larger than that of TCPP-PEG$_{2K}$ (412.2%ID h g^{-1}) at 4 h p.i. (Figure S14e, Supporting Information). The elevated tumor uptake for TCPP-PEG$_{30k}$ was attributed to the enhanced blood circulation. The tumor-targeting efficiencies of the TCPP-PEG$_{30K}$ were determined to be 5.6 ± 1.5 and 6.9 ± 1.1%ID g^{-1} at 4 and 24 h p.i., respectively, slightly higher than TCPP-PEG$_{10K}$ (4.2 ± 0.7 and 4.7 ± 0.35%ID g^{-1}), but much higher than TCPP-PEG$_{2K}$ (2.3 ± 0.57 and 2.2 ± 0.50%ID g^{-1}) and TCPP-PEG$_{5K}$ (2.4 ± 0.57 and 2.8 ± 0.48%ID g^{-1}) nanoparticles (Figure 3c). Such an efficient passive tumor homing of the nanoparticles could be attributed to the EPR effect of 4T1 tumors through the long blood circulation.[12]

Next, we carefully investigated the clearance behaviors of these various TCPP-PEG nanoparticles. For TCPP-PEG$_{30K}$
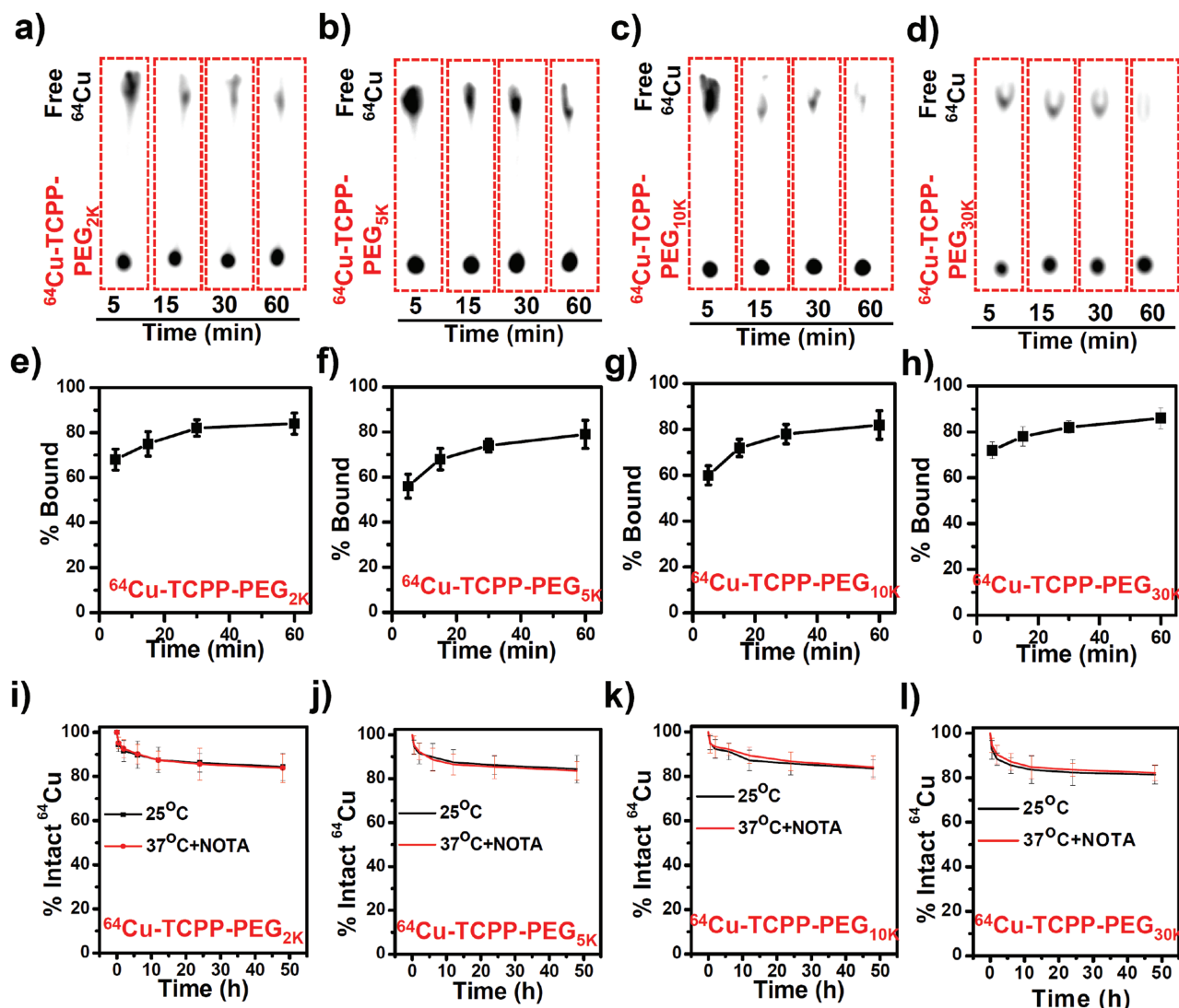
Figure 2. Intrinsically ^{64}Cu-labeled TCPP-PEG nanoparticles. a–d) Thin-layer chromatography (TLC) plates of TCPP-PEG nanoparticles at various time points after mixing ^{64}Cu with TCPP-PEG nanoparticles: (a) TCPP-PEG$_{2K}$, (b) TCPP-PEG$_{5K}$, (c) TCPP-PEG$_{10K}$, and (d) TCPP-PEG$_{30K}$. e–h) Quantified labeling yield of ^{64}Cu on TCPP-PEG nanoparticles at various time points after incubation ($n = 3$): (e) TCPP-PEG$_{2K}$, (f) TCPP-PEG$_{5K}$, (g) TCPP-PEG$_{10K}$, and (h) TCPP-PEG$_{30K}$. i–l) Stability test of ^{64}Cu labeling on TCPP-PEG nanoparticles after incubation in serum with or without NOTA competitive reaction at 37 °C for different periods of time: (i) TCPP-PEG$_{2K}$, (j) TCPP-PEG$_{5K}$, (k) TCPP-PEG$_{10K}$, and (l) TCPP-PEG$_{30K}$.

nanoparticles, only radioactive signal in the bladder in the first 30 min was observed. However, strong PET signals were found in the kidneys and bladder in the initial 6 h time point for the lower molecular weight of TCPP-PEG nanoparticles (2, 5, and 10 K) after i.v. injection (Figure 3a and Figure S15a (Supporting Information)), proving that the majority of them underwent clearance. However, their rate of kidney filtration varied between the nanoparticles. Detailed biodistribution of ^{64}Cu-TCPP-PEG nanoparticles in the left kidney and bladder was summarized in Figure S15b,c (Supporting Information). In the initial 4 h, all the TCPP-PEG nanoparticles showed high signal in bladder with up to 172.1 ± 32.4%ID g^{-1}, except TCPP-PEG$_{30K}$ nanoparticles (9.7 ± 1.4%ID g^{-1}). All the samples showed high signal in the kidneys in the initial time points, indicating that our synthesized TCPP-PEG nanoparticles with small HD sizes can pass through the kidneys

for rapid clearance. As expected, the radioactive signal of ^{64}Cu-TCPP-PEG in the kidneys with lower molecular weights (2 and 5 K) was stronger than that with larger molecular weights (for example, 10 and 30 K) at all time points. In order to investigate the renal-clearable TCPP-PEG nanoparticles, a unilateral ureteral obstruction (UUO) mouse model was used, which was generated by complete ligation of the left ureter of the mouse while the right ureter was kept intact[13] (Figure S16, Supporting Information). After i.v. injection of the ^{64}Cu-TCPP-PEG$_{2K}$ nanoparticles, the obstructed left kidney exhibited dramatically reduced radioactivity signals compared to the contralateral right kidney (RK) in UUO mice in the first half an hour, but much higher than the RK at 1 and 2 h time points p.i. Such a diminished accumulation of contrast agent in the UUO kidney indicated that the blood perfusion had been dramatically reduced upon obstruction, which was consistent with
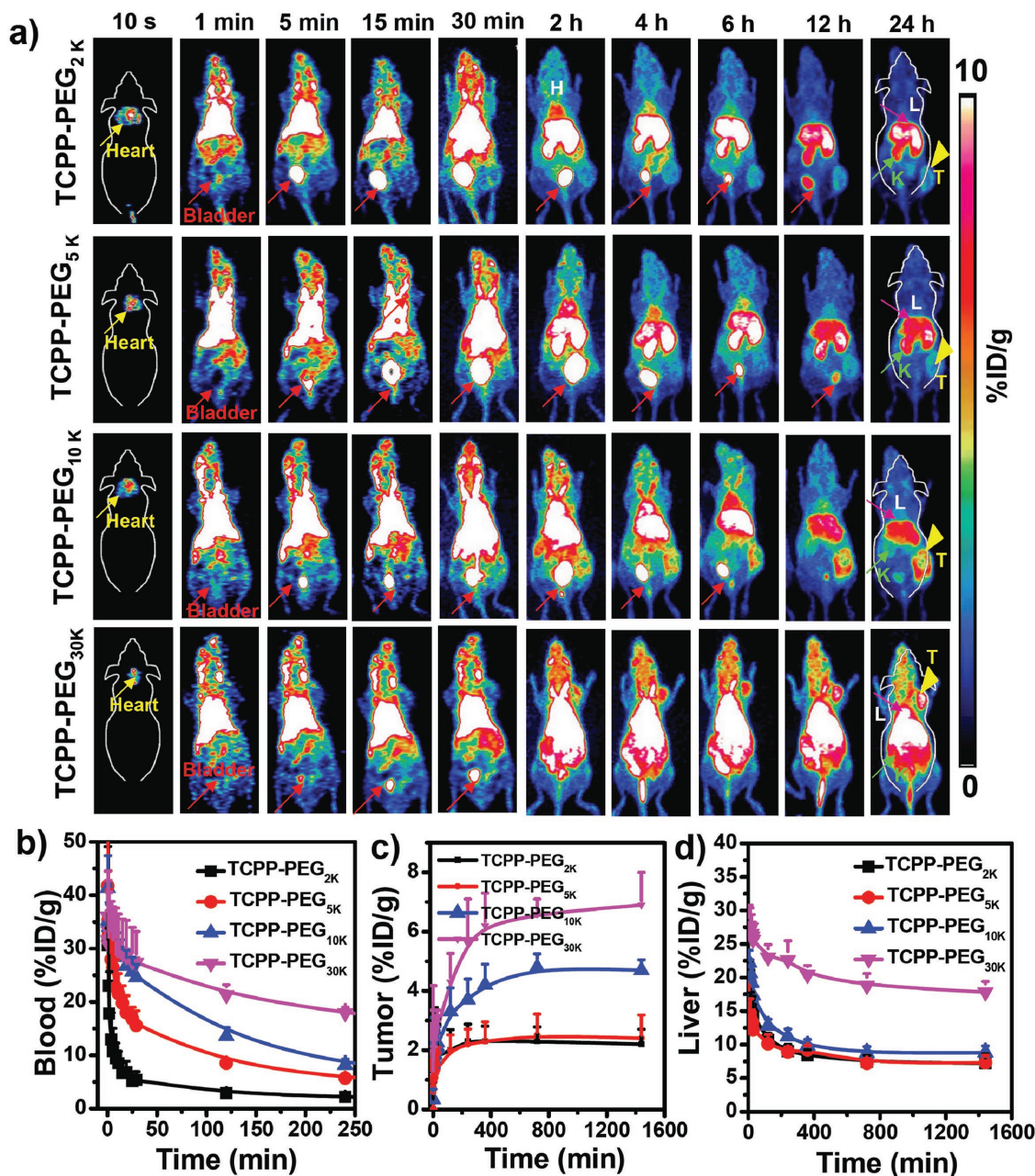
ADVANCED
SCIENCE NEWS
www.advancedsciencenews.com

ADVANCED
FUNCTIONAL
MATERIALS
www.afm-journal.de

Figure 3. In vivo PET imaging: a) PET images of 4T1 tumor-bearing mice taken at various time points (10 s, 1 min, 5 min, 15 min, 30 min, 2 h, 4 h, 6 h, 12 h, and 24 h) postinjection of ^{64}Cu-TCPP-PEG$_{2K}$, ^{64}Cu-TCPP-PEG$_{5K}$, ^{64}Cu-TCPP-PEG$_{10K}$, and ^{64}Cu-TCPP-PEG$_{30K}$ nanoparticles. Liver (L), kidneys (K), heart, and bladder are indicated in each figure. Tumor (T) is indicated by yellow arrowheads. b–d) Time-activity curves of ^{64}Cu-TCPP-PEG (2, 5, 10, and 30 K) in different major organs of (b) blood, (c) tumor, and (d) liver.

previous findings obtained by SPECT imaging of the UUO mice.[14] Importantly, these finding suggested that glomerular filtration was likely a major clearance route for the small size of nanoparticles, such as TCPP-PEG$_{2K}$ nanoparticles.

The mouse liver also showed the same phenomenon that signal of radioactivity after i.v. injection of TCPP-PEG nanoparticles with the molecular weight less than 10 K decreased with the increasing time (Figure 3d and Figure S17 (Supporting Information)). Uptakes in the liver were 7.2 ± 1.4%ID g^{-1} for TCPP-PEG$_{2K}$, 7.3 ± 1.1%ID g^{-1} for

TCPP-PEG$_{5K}$, and 8.8 ± 1.98%ID g^{-1} for TCPP-PEG$_{10K}$ at 24-h time point p.i. Despite high tumor uptake for TCPP-PEG$_{30K}$ nanoparticles, most of them were still deposited in the liver for a long time (up to 17.8 ± 1.6%ID g^{-1}), which was 2 times higher than any other smaller molecular weight of TCPP-PEG nanoparticles. Finally, the ^{64}Cu radionuclide dose left in the body was found to be 20.5, 24.2, 28.5, and 50.8%ID for TCPP-PEG$_{2K}$, TCPP-PEG$_{5K}$, TCPP-PEG$_{10K}$, and TCPP-PEG$_{30K}$ nanoparticles 24 h after i.v. injection of ^{64}Cu-TCPP-PEG nanoparticles (Figure S18, Supporting Information). Considering the balance

**ADVANCED
SCIENCE NEWS**
www.advancedsciencenews.com

**ADVANCED
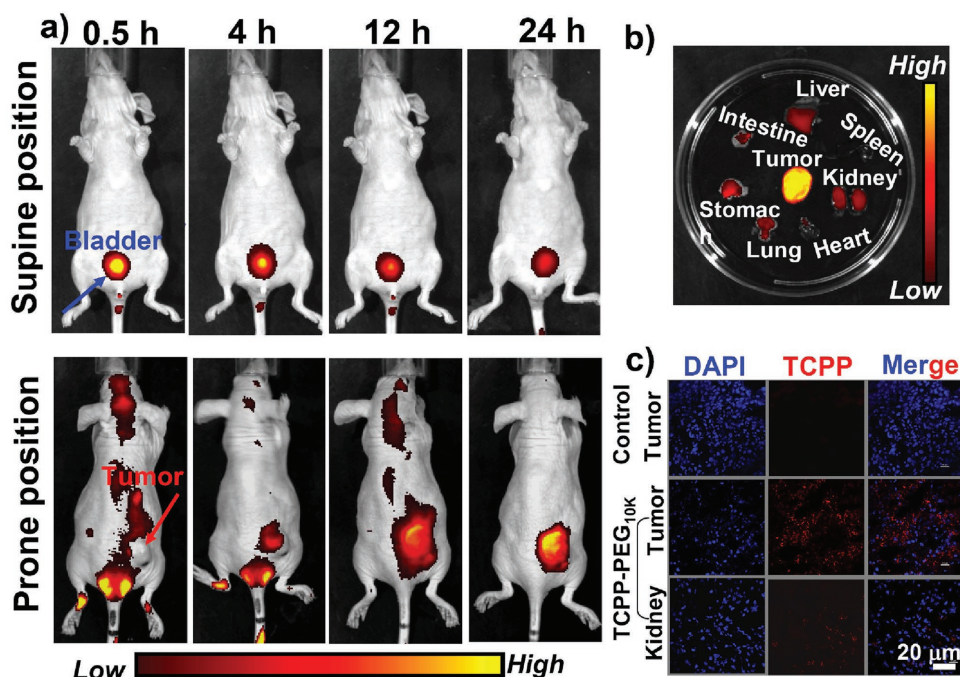FUNCTIONAL
MATERIALS**
www.afm-journal.de

Figure 4. In vivo and ex vivo fluorescence imaging: a,b) In vivo fluorescence images of 4T1 tumor-bearing nude mice taken at different time points postinjection of TCPP-PEG$_{10K}$ nanoparticles with prone (top) and supine (bottom). (b) Ex vivo fluorescence images of major organs and tumor dissected from mice injected with TCPP-PEG$_{10K}$ nanoparticles at 24 h p.i. c) Confocal images of tumor and kidney tissues after i.v. injection TCPP-PEG$_{10K}$ nanoparticles or not at 24 h p.i. Red color represents the fluorescence signal from TCPP molecule.

of clearance and tumor uptake, TCPP-PEG$_{10K}$ nanoparticles were chosen for the following investigation.

In vivo fluorescence imaging conducted at different time points after i.v. injection of TCPP-PEG$_{10K}$ nanoparticles (1 mg mL^{-1}, 200 µL) allowed us to further investigate the behaviors of clearance and tumor uptake (**Figure** 4a, supine position). The TCPP-PEG$_{10K}$ nanoparticles were rapidly excreted into the bladder, and the fluorescence intensity of the bladder area reached its maximum in the initial half hour p.i. In the remaining time points, we still found strong signal in the bladder, further confirming that TCPP-PEG$_{10K}$ nanoparticles were clearable after i.v. injection. The fluorescence signal from the TCPP-PEG$_{10K}$ nanoparticles also increased in the tumor over time, with the prominent uptake at 24 h p.i. (Figure 4a, prone position; Figure S19, Supporting Information), which was consistent with the above PET imaging results. Ex vivo imaging at 24 h p.i. revealed that TCPP primarily accumulated in the tumor, liver, spleen, and kidneys (Figure 4b and Figure S20 (Supporting Information)). To further confirm the tumor accumulation of TCPP-PEG$_{10K}$ nanoparticles, tumor tissues were sectioned and imaged by confocal microscopy. As shown in Figure 4c, strong red fluorescence was clearly visualized in tumor slices, verifying the prominent uptake of TCPP-PEG$_{10K}$ nanoparticles in the tumor, while no fluorescence signal was detected from the tumor tissues devoid of TCPP-PEG$_{10K}$ nanoparticles when using the same imaging condition. The results clearly indicated the efficient tumor passive uptake of our TCPP-PEG$_{10K}$ nanoparticles. Next, we examined the potential toxicities associated with the renal clearance of our nanoparticles. The kidneys were sectioned

and investigated for the nanoparticle uptake and cellular toxicity. Strong fluorescence signal was observed from the kidney tissues 24 h p.i. (Figure 4c), indicating that the nanoparticles passed through the kidneys for clearance. Moreover, the tissues were devoid of any noticeable abnormalities or lesions, confirming the nontoxicity of our TCPP-PEG$_{10K}$ nanoparticles with clearance behavior (Figure S21, Supporting Information).

TCPP porphyrins have been widely used as a photosensitizer for photodynamic cancer therapy and could effectively generate singlet oxygen under light irradiation.[15] It motivated us to investigate the PDT effect of TCPP-PEG$_{10K}$ nanoparticles. Compared with free TCPP, TCPP-PEG$_{10K}$ nanoparticles showed a slightly higher efficiency of light-triggered singlet oxygen production at the same TCPP concentrations (Figure S22, Supporting Information), which was attributed to the better solubility after modification, indicating that the synthesized TCPP-PEG$_{10K}$ nanoparticles could be a better agent for PDT. No significant cytotoxicity was observed for all TCPP-PEG nanoparticles, even at high concentrations of up to 20×10^{-6} M (Figure S23, Supporting Information). The intracellular uptake of our TCPP-PEG$_{10K}$ nanoparticles was also time-dependent (Figure S24, Supporting Information). Next, we used TCPP-PEG$_{10K}$ nanoparticles as a photodynamic agent for in vitro cancer therapy under laser irradiation. The majority of 4T1 cells were destroyed after incubation with 5×10^{-6} M of TCPP-PEG$_{10K}$ nanoparticles and exposure to the 658 nm laser (Figure S25a, Supporting Information). The PDT effects of TCPP-PEG$_{10K}$ nanoparticles on 4T1 cells were further investigated using Trypan blue staining. Upon laser irradiation, most cells incubated with TCPP-PEG$_{10K}$ nanoparticles were damaged, as

ADVANCED
SCIENCE NEWS
www.advancedsciencenews.com

ADVANCED
FUNCTIONAL
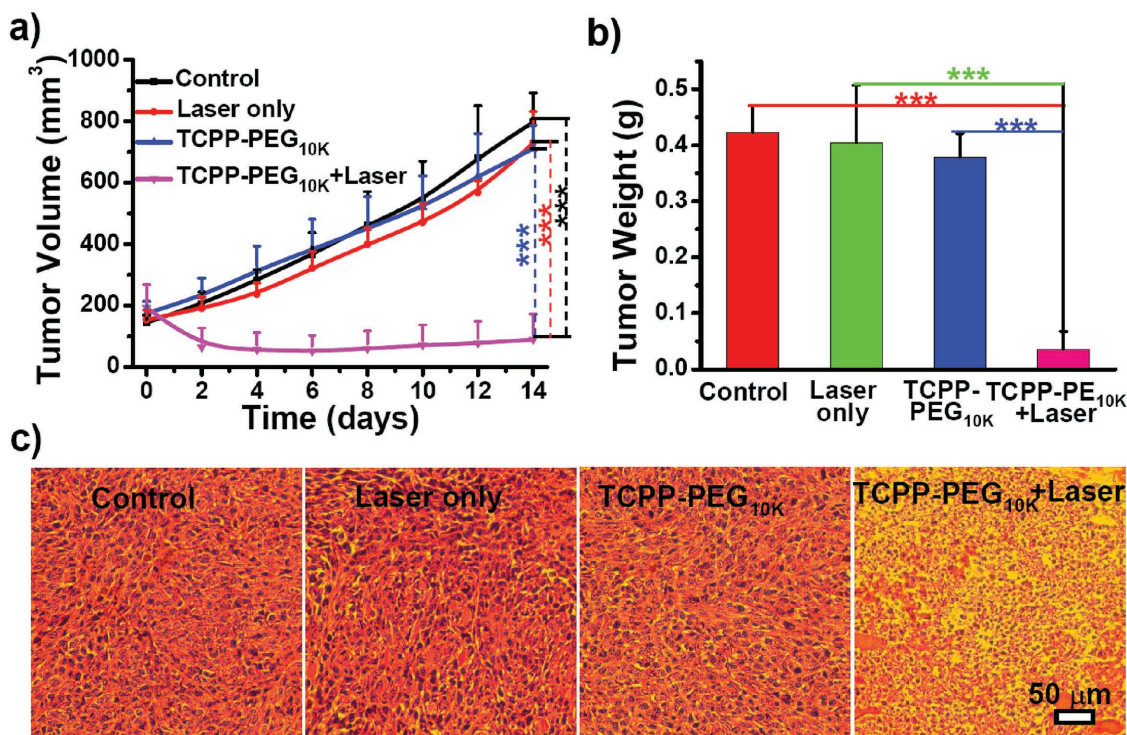MATERIALS
www.afm-journal.de

Figure 5. In vivo PDT. a) Tumor growth curves of different groups of mice after various treatments indicated. For the treatment group, four mice injected with TCPP-PEG$_{10K}$ nanoparticles at 24 h p.i. were exposed to the 658 nm laser (50 mW cm^{-2}, 30 min). Other three groups of mice were used as controls: untreated (Control, $n = 4$); laser only without TCPP-PEG$_{10K}$ injection (Laser only, $n = 4$); TCPP-PEG$_{10K}$ nanoparticles injected but without laser irradiation (TCPP-PEG$_{10K}$, $n = 4$). Error bars were based on SD. b) Tumor weight of different groups taken at the 14th d. c) H&E-stained tumor slices collected from different groups of mice on the following day after various treatments. Statistical analysis was performed using the Student's two-tailed t test: *$p < 0.05$, **$p < 0.01$, and ***$p < 0.001$. Renal-clearable PEGylated porphyrin nanoparticles for image-guided photodynamic cancer therapy.

indicated by the intense homogeneous blue color (Figure S25b, Supporting Information). The amount of cell death gradually increased upon increasing the concentrations of TCPP-PEG$_{10K}$ nanoparticles. These findings altogether revealed that TCPP-PEG$_{10K}$ nanoparticles hold great promise as an effective photodynamic agent for in vivo tumor therapy.

Encouraged by the high PDT efficiency in vitro and the efficient passive tumor targeting of TCPP-PEG$_{10K}$ nanoparticles, in vivo PDT studies were performed to evaluate the anticancer efficacy of TCPP-PEG$_{10K}$ nanoparticles. For the PDT group ($n = 4$), the mice were i.v. injected with TCPP-PEG$_{10K}$ nanoparticles (200 µL, 1 mg mL^{-1}) and then irradiated for 30 min with the 658 nm laser at 50 mW cm^{-2} after 24 h p.i. As illustrated in **Figure 5**a, TCPP-PEG$_{10K}$ nanoparticle-mediated PDT can significantly inhibit tumor growth, whereas laser irradiation alone or PBS injection with laser irradiation did not affect the tumor growth. These results suggest that TCPP-PEG$_{10K}$ nanoparticles are a powerful agent for in vivo PDT of cancer (Figure 5b). To further understand the PDT effects after various treatments down to the cellular level, hematoxylin and eosin (H&E) staining was utilized to study the morphology and apoptosis of tumor cells after 2 d posttreatment. The results indicated that most cancer cells were completely destroyed in the TCPP-PEG$_{10K}$ nanoparticles with laser treatment group (Figure 5c), while cells in the other three control groups mainly retained their normal morphology, further confirming the efficacy of TCPP-PEG$_{10K}$ polymer for in vivo photodynamic ablation of cancer.

3. Conclusion

In summary, our study introduced a simple method to synthesize PEGylated TCPP porphyrin nanoparticles and employed noninvasive dynamic PET imaging to investigate the balance of the renal clearance and tumor uptake behaviors. We found that PEG with larger molecular weights was better for tumor uptake and the lower ones were suitable for renal clearance. Considering this balance, TCPP-PEG$_{10K}$ nanoparticles were the most suitable model to investigate clearance and tumor uptake. In vitro and in vivo PDT experiments were carried out which led to excellent therapeutic efficacy. Therefore, our work presented a simple fabrication method for selection of biocompatible multifunctional TCPP-PEG-based theranostic agents with renal clearance behavior, which highlights the clinical application potential of TCPP-PEG as theranostic probes for imaging-guided cancer therapy.

4. Experimental Section

Materials: mTCPP and dimethyl sulfoxide (DMSO) were obtained from Frontier Scientific, Inc. (Logan, UT, USA). PEG$_{2K}$, PEG$_{5K}$, PEG$_{10K}$, and PEG$_{30K}$ were obtained from Biomatrik Co., Ltd. (Jiaxing, China) with the molecular weight of 2, 5, 10, and 30 kDa, respectively. EDC and N-hydroxysulfosuccinimide (Sulfo-NHS) were obtained from Sigma-Aldrich. Deionized water used in our experiments was obtained from a Milli-Q water system.

**ADVANCED
SCIENCE NEWS**
www.advancedsciencenews.com

**ADVANCED
FUNCTIONAL
MATERIALS**
www.afm-journal.de

Synthesis of TCPP-PEG Nanoparticles: TCPP-PEG nanoparticles with various molecular weights were synthesized according to the protocol reported previously with slight modification.[10] First, 10 µmol of TCPP was mixed with 5 µmol of EDC and 5 µmol of Sulfo-NHS in 100 µL anhydrous DMSO for 0.5 h at room temperature. Then, PEG with different molecular weight (2, 5, 10, and 30 K) in 2 mL water was slowly added to the above-activated TCPP molecules. The molar ratio of PEG-NH$_2$:TCPP:EDC:NHS was 1:2:1:1. After reacting for 24 h at room temperature, excess TCPP molecules, catalysts, and DMSO were removed by Millipore filters with different molecular weight cut off. Afterward, TCPP-PEG$_{2K}$, TCPP-PEG$_{5K}$, TCPP-PEG$_{10K}$, and TCPP-PEG$_{30K}$ nanoparticles in water were obtained and stored at −4 °C for future use. The concentration of TCPP-PEG nanoparticles was defined by TCPP content.

Characterization: TEM images of the nanoparticles were obtained using an FEI Tecnai F30 transmission electron microscope at an acceleration voltage of 300 kV. UV–vis–near infrared absorbance (NIR) spectra were obtained with PerkinElmer Lambda 750 UV-vis-NIR spectrophotometer. Fluorescence spectra of different samples were obtained on a FluoroMax 4 luminescence spectrometer (HORIBA Jobin Yvon). The HDs of TCPP-PEG nanoparticles were determined by a ZetaSizer Nano-ZS (Malvern Instruments, UK). MALDI-TOF spectra of TCPP-PEG nanoparticles were obtained from MDS SCIEX 4800 MALDI TOF/TOF (Applied Biosystems, Foster City, CA, USA). ^{1}H NMR spectra were recorded on a 400 MHz NMR spectrometer (INOVA-400) at 25 °C with CDCl$_3$ as the solvent and tetramethylsilane as the internal standard. FTIR absorption spectra of the nanoparticles were recorded by using a Nicolet 6700 spectrometer at 4 cm^{-1} resolution, over the wavenumber range 400–4000 cm^{-1}.

Tumor Models: All animal studies were conducted under a protocol approved by the University of Wisconsin Institutional Animal Care and Use Committee. The 4T1 subcutaneous xenografts were generated by subcutaneous injection of 1×10^6 cells in ≈50 µL RMPI-1640 medium onto the back of each female BALB/c mice. In order to investigate the optical imaging of TCPP-PEG nanoparticles, female nude mice were employed. To develop the tumor model, 1×10^6 4T1 cells in ≈50 µL PBS were injected onto the back of female nude mice. The mice were used when tumor volumes reached about ≈150 mm^3.

^{64}Cu Labeling and Animal Model for Dynamic PET Imaging: ^{64}Cu^{2+} was produced with an onsite cyclotron (GE PET trace). Briefly, ^{64}CuCl$_2$ (≈150 MBq) was diluted in 300 µL of 0.1 M sodium acetate buffer (pH 5.5) and mixed with 100 µL various kinds of TCPP-PEG nanoparticles (0.1 mg mL^{-1}). The reaction was conducted at 37 °C for 1 h with constant shaking. The labeling yield was determined by thin-layer chromatography at different time points. The resulting ^{64}Cu-TCPP-PEG (2, 5, 10, and 30 K) nanoparticles were purified using PD-10 columns with PBS as the mobile phase.

The serum stability study was carried out to ensure ^{64}Cu^{2+} was stably attached on TCPP-PEG nanoparticles. ^{64}Cu-TCPP-PEG nanoparticles with various molecule weights were incubated in complete serum at 37 °C for up to 48 h. At different time points, portions of the mixture were sampled and filtered through molecular weight cut-off (MWCO) filters with different molecular weights. The retained (i.e., intact) ^{64}Cu^{2+} on ^{64}Cu-TCPP-PEG nanoparticles was calculated using the equation (radioactivity on filter/total sampled radioactivity × 100%).

In order to investigate the serum stability of nanoparticles, not only the stability in mouse serum containing warm media (37 °C) was investigated, but NOTA as the stronger challenge chelator to remove unstable ^{64}Cu-labeled TCPP-PEG nanoparticles was also added. NOTA (20 µL) with the concentration of 1×10^{-3} M was added into 250 µL of ^{64}Cu-TCPP-PEG (≈300 µCi) in complete mouse serum solution (pH 7) at 37 °C under constant shaking (≈600 rpm) for 48 h. At each time point, 25 µL of the mixture was taken out and resuspended in 100 µL of NaOAc buffer. A filter was used to separate potential ^{64}Cu-NOTA from ^{64}Cu-TCPP-PEG nanoparticles. The radioactivity of ^{64}Cu-NOTA and ^{64}Cu-TCPP-PEG nanoparticles was measured by using a gamma counter (PerkinElmer). ^{64}Cu-TCPP-PEG with various molecule weights was found

to be highly stable in warm mouse serum for up to 48 h even with NOTA challenge.

In vivo positron emission tomography (PET) imaging studies were performed in a microPET/microCT Inveon rodent model scanner (Siemens Medical Solutions USA, Inc.). For dynamic PET studies, BALB/c mice planted with 4T1 tumors were anesthetized under isoflurane and their tail vein catheterized. Following this, animals were put in the scanner in a prone position and simultaneously with the injection of ≈300 µCi of various kinds of TCPP-PEG nanoparticles (^{64}Cu-TCPP$_{2K}$, ^{64}Cu-TCPP$_{5K}$, ^{64}Cu-TCPP$_{10K}$, and ^{64}Cu-TCPP$_{30K}$), and a 30-min emission scan was acquired. List mode files were framed into 28 frames: 6×10, 6×30, 6×60, and 10×120 s. Another five additional static PET scans at 2, 4, 6, 12, and 24 h p.i. of the nanoparticles were acquired. Data acquisition, image reconstruction, and region of interest (ROI) analysis of the PET data were performed as described previously.[16] After the PET scans at 24 h, ex vivo biodistribution studies carried out to ensure the %ID g^{-1} values determined by PET imaging truly represented the radioactivity distribution in tumor-bearing mice. Mice were euthanized, and blood, tumor, and major organs/tissues were collected and wet-weighed. The radioactivity in the tissue was measured using a gamma-counter (PerkinElmer, USA) and presented as %ID g^{-1} (mean ± SD).

UUO Model: Mice were anesthetized with 2% isoflurane, and the left kidney was exposed through the site of the incision. The ureter was obstructed completely near the renal pelvis using a 4-0 silk tie suture at two points. After 2 d, in vivo dynamic PET imaging studies were performed in a microPET/microCT Inveon rodent model scanner after i.v. injection of ≈300 µCi of ^{64}Cu-TCPP-PEG$_{2K}$ nanoparticles at various time points. Data acquisition, image reconstruction, and ROI analysis of the PET data were performed as described above.

In Vivo Fluorescence Imaging of TCPP-PEG$_{10K}$ Nanoparticles: For in vivo imaging, 200 µL of TCPP-PEG$_{10K}$ nanoparticles (1 mg mL^{-1}) was i.v. injected into each mouse. In vivo fluorescence imaging was conducted using an IVIS Spectrum fluorescence imager. Mice were imaged using a 675 nm/740 nm excitation/emission filter pair under automatic exposure settings, and fluorescence signal was displayed as radiant efficiency. The mice were sacrificed at 24 h after i.v. injection, with their major organs including the tumor, liver, heart, lung, spleen, and kidneys collected for ex vivo imaging. Finally, the tumor and kidney tissues were frozen in optimum cutting temperature solution (SACURA, USA) medium and cut into 8 µm slices for confocal imaging.

Single Oxygen Detection: The method for singlet oxygen detection was based on the protocol reported previously.[17] In brief, 100 mg of Singlet oxygen sensor green or SOSG (Molecular Probes, USA) was dissolved in 330 mL of methanol to obtain the stock solution of SOSG (0.5×10^{-3} M). Then, 10 µL of SOSG was added to 2 mL of TCPP-PEG$_{10K}$ nanoparticles solution containing 0.2 mg TCPP. Next, the sample was irradiated by a 658 nm laser at a power density of 20 mW cm^{-2}. The same concentration of free TCPP molecules dissolved in DMSO/water under laser irradiation was used as the control. The fluorescence intensity of SOSG was measured with an excitation wavelength of 494 nm.

Cell Culture Experiment: Murine breast cancer 4T1 cells were obtained from the American Type Culture Collection and cultured at 37 °C under 5% CO$_2$. All cell culture-related reagents were purchased from Invitrogen. 4T1 cells were cultured in normal RPMI-1640 medium containing 10% fetal bovine serum and 1% penicillin/streptomycin. Cells were seeded into 96-well plates at a density of 1×10^4 cells per well and incubated with different concentrations of TCPP-PEG$_{10K}$ nanoparticles for 24 h. Relative cell viabilities were determined by the standard methyl thiazolyl tetrazolium (MTT) assay.

To examine the cellular uptake of TCPP-PEG$_{10K}$ nanoparticles, 4T1 cells were plated in 35 mm dish with 14 mm bottom well (1×10^5 cells per well) for 24 h. After adhesion, TCPP-PEG$_{10K}$ nanoparticles were added into the wells at the concentration of 5×10^{-6} M (TCPP) and cultured for different time periods (1, 3, 6, and 24 h). After washing 3 times with PBS (pH = 7.4), cells were fixed by 4% paraformaldehyde and labeled with 4′, 6-diamidino-2-phenylindole before imaging with a

Nikon A1RS confocal microscope, and imaging analysis was performed using the NIS-Elements Ar with Deconvolution package.

In Vitro PDT: For in vitro PDT, 4T1 cells (1×10^4) were seeded in 96-well plates and added with TCPP-PEG$_{10K}$ nanoparticles at various concentrations. After incubation for 12 h, the experimental groups were exposed to 658 nm laser irradiation under a power density of 20 mW cm^{-2} for 15 min, while the control groups were still cultured in dark. Afterward, all samples were incubated in the dark for another 12 h. In order to determine relative cell viabilities after various treatments, the MTT assay was carried out following the standard protocol. After laser irradiation, cells were washed with PBS and stained with 0.4% Trypan blue (Sigma-Aldrich) before imaged by a Nikon Elipse Ti microscope.

In Vivo PDT: To develop the tumor model, 4T1 cells (1×10^6) suspended in 50 µL of PBS were subcutaneously injected into the back of each BALB/c mouse. After the tumor volume reached ≈150 mm^3, mice were randomly divided into four groups ($n = 4$ per group) for various treatments: (i) Control; (ii) Laser only; (iii) TCPP-PEG$_{10K}$ nanoparticles i.v. injection; and (iv) TCPP-PEG$_{10K}$ nanoparticles i.v. injection + Laser. TCPP-PEG$_{10K}$ nanoparticles, at a dose of 10 mg kg^{-1}, were i.v. injected into mice bearing 4T1 tumors. PDT treatments were conducted 24 h later, with the 658 nm laser at the power density of 50 mW cm^{-2} for 30 min. The tumor sizes were measured by a caliper every other day and calculated as the volume = (tumor length) × (tumor width)^2/2. Relative tumor volumes were calculated as V/V_0 (V_0 was the initial tumor volume). Two d after treatment, the tumors in each group were dissected to make paraffin sections for further H&E staining.

Supporting Information

Supporting Information is available from the Wiley Online Library or from the author.

Conflict of Interest

The authors declare no conflict of interest.

[1] a) C. Holohan, S. Van Schaeybroeck, D. B. Longley, P. G. Johnston, *Nat. Rev. Cancer* **2013**, *13*, 714; b) R. L. Siegel, K. D. Miller, A. Jemal, *Ca-Cancer J. Clin.* **2015**, *65*, 5.

[2] a) L. Cheng, C. Wang, L. Feng, K. Yang, Z. Liu, *Chem. Rev.* **2014**, *114*, 10869; b) X. Huang, I. H. El-Sayed, W. Qian, M. A. El-Sayed, *J. Am. Chem. Soc.* **2006**, *128*, 2115; c) D. P. O'Neal, L. R. Hirsch, N. J. Halas, J. D. Payne, J. L. West, *Cancer Lett.* **2004**, *209*, 171; d) D. E. Dolmans, D. Fukumura, R. K. Jain, *Nat. Rev. Cancer* **2003**, *3*, 380; e) J. F. Lovell, T. W. Liu, J. Chen, G. Zheng, *Chem. Rev.* **2010**, *110*, 2839.

[3] a) K. K. Ng, G. Zheng, *Chem. Rev.* **2015**, *115*, 11012; b) S. S. Lucky, K. C. Soo, Y. Zhang, *Chem. Rev.* **2015**, *115*, 1990; c) D.-E. Lee, H. Koo, I.-C. Sun, J. H. Ryu, K. Kim, I. C. Kwon, *Chem. Soc. Rev.* **2012**, *41*, 2656; d) A. Kamkaew, S. H. Lim, H. B. Lee, L. V. Kiew, L. Y. Chung, K. Burgess, *Chem. Soc. Rev.* **2013**, *42*, 77; e) D. Gao, L. Gao, C. Zhang, H. Liu, B. Jia, Z. Zhu, F. Wang, Z. Liu, *Biomaterials* **2015**, *53*, 229; f) C. Qian, J. Yu, Y. Chen, Q. Hu, X. Xiao, W. Sun, C. Wang, P. Feng, Q.-D. Shen, Z. Gu, *Adv. Mater.* **2016**, *28*, 3313; g) Z. Sheng, D. Hu, M. Zheng, P. Zhao, H. Liu, D. Gao, P. Gong, G. Gao, P. Zhang, Y. Ma, *ACS Nano* **2014**, *8*, 12310; h) L. Cheng, J. Liu, X. Gu, H. Gong, X. Shi, T. Liu, C. Wang, X. Wang, G. Liu, H. Xing, *Adv. Mater.* **2014**, *26*, 1886.

[4] H. S. Choi, J. V. Frangioni, *Mol. Imaging* **2010**, *9*, 291.

[5] a) H. Soo Choi, W. Liu, P. Misra, E. Tanaka, J. P. Zimmer, B. Itty Ipe, M. G. Bawendi, J. V. Frangioni, *Nat. Biotechnol.* **2007**, *25*, 1165; b) C. Zhou, M. Long, Y. Qin, X. Sun, J. Zheng, *Angew. Chem. Int. Ed.* **2011**, *50*, 3168; c) C. H. J. Choi, J. E. Zuckerman, P. Webster, M. E. Davis, *Proc. Natl. Acad. Sci. USA* **2011**, *108*, 6656; d) X.-D. Zhang, J. Chen, Y. Min, G. B. Park, X. Shen, S.-S. Song, Y.-M. Sun, H. Wang, W. Long, J. Xie, K. Gao, L. Zhang, S. Fan, F. Fan, U. Jeong, *Adv. Funct. Mater.* **2014**, *24*, 1718; e) J. Liu, P. Wang, X. Zhang, L. Wang, D. Wang, Z. Gu, J. Tang, M. Guo, M. Cao, H. Zhou, Y. Liu, C. Chen, *ACS Nano* **2016**, *10*, 4587; f) J. Liu, M. Yu, C. Zhou, S. Yang, X. Ning, J. Zheng, *J. Am. Chem. Soc.* **2013**, *135*, 4978; g) X.-D. Zhang, D. Wu, X. Shen, P.-X. Liu, F.-Y. Fan, S.-J. Fan, *Biomaterials* **2012**, *33*, 4628.

[6] a) F. Lux, A. Mignot, P. Mowat, C. Louis, S. Dufort, C. Bernhard, F. Denat, F. Boschetti, C. Brunet, R. Antoine, P. Dugourd, S. Laurent, L. V. Elst, R. Muller, L. Sancey, V. Josserand, J.-L. Coll, V. Stupar, E. Barbier, C. Rémy, A. Broisat, C. Ghezzi, G. Le Duc, S. Roux, P. Perriat, O. Tillement, *Angew. Chem. Int. Ed.* **2011**, *50*, 12299; b) W. Jiang, Y. S. KimBetty, J. T. Rutka, C. W. ChanWarren, *Nat. Nanotechnol.* **2008**, *3*, 145; c) X. Huang, F. Zhang, L. Zhu, K. Y. Choi, N. Guo, J. Guo, K. Tackett, P. Anilkumar, G. Liu, Q. Quan, H. S. Choi, G. Niu, Y.-P. Sun, S. Lee, X. Chen, *ACS Nano* **2013**, *7*, 5684; d) S. Tang, C. Peng, J. Xu, B. Du, Q. Wang, R. D. Vinluan, M. Yu, M. J. Kim, J. Zheng, *Angew. Chem. Int. Ed.* **2016**, *128*, 16273.

[7] M.-k. Kim, H.-J. Jeong, C.-H. K. Kao, Z. Yao, D. S. Paik, J. E. Pie, H. Kobayashi, T. A. Waldmann, J. A. Carrasquillo, C. H. Paik, *Nucl. Med. Biol.* **2002**, *29*, 139.

[8] F. Liu, X. He, H. Chen, J. Zhang, H. Zhang, Z. Wang, *Nat. Commun.* **2015**, *6*, 8003.

[9] J. Xie, G. Liu, H. S. Eden, H. Ai, X. Chen, *Acc. Chem. Res.* **2011**, *44*, 883.

[10] H. Huang, R. Hernandez, J. Geng, H. Sun, W. Song, F. Chen, S. A. Graves, R. J. Nickles, C. Cheng, W. Cai, J. F. Lovell, *Biomaterials* **2016**, *76*, 25.

[11] a) Y. Zhang, M. Jeon, L. J. Rich, H. Hong, J. Geng, Y. Zhang, S. Shi, T. E. Barnhart, P. Alexandridis, J. D. Huizinga, M. Seshadri, W. Cai, C. Kim, J. F. Lovell, *Nat. Nanotechnol.* **2014**, *9*, 631; b) M. Lortie, R. S. B. Beanlands, K. Yoshinaga, R. Klein, J. N. DaSilva, R. A. deKemp, *Eur. J. Nucl. Med. Mol. Imaging* **2007**, *34*, 1765.

[12] a) V. P. Chauhan, T. Stylianopoulos, J. D. Martin, Z. Popovic, O. Chen, W. S. Kamoun, M. G. Bawendi, D. Fukumura, R. K. Jain,

**ADVANCED
SCIENCE NEWS**
www.advancedsciencenews.com

**ADVANCED
FUNCTIONAL
MATERIALS**
www.afm-journal.de

Nat. Nanotechnol. **2012**, *7*, 383; b) L. Cheng, K. Yang, Q. Chen, Z. Liu, *ACS Nano* **2012**, *6*, 5605.

[13] a) M. Yu, J. Zhou, B. Du, X. Ning, C. Authement, L. Gandee, P. Kapur, J.-T. Hsieh, J. Zheng, *Angew. Chem. Int. Ed.* **2016**, *55*, 2787; b) M. N. Tantawy, R. Jiang, F. Wang, K. Takahashi, T. E. Peterson, D. Zemel, C.-M. Hao, H. Fujita, R. C. Harris, C. C. Quarles, T. Takahashi, *BMC Nephrol.* **2012**, *13*, 168.

[14] F. J. Penna, J. S. Chow, B. J. Minnillo, C. C. Passerotti, C. E. Barnewolt, S. T. Treves, F. H. Fahey, P. S. Dunning, D. A. Freilich, A. B. Retik, H. T. Nguyen, *J. Urol.* **2011**, *185*, 2405.

[15] R. J. Fiel, N. Datta-Gupta, E. H. Mark, J. C. Howard, *Cancer Res.* **1981**, *41*, 3543.

[16] L. Cheng, S. Shen, S. Shi, Y. Yi, X. Wang, G. Song, K. Yang, G. Liu, T. E. Barnhart, W. Cai, Z. Liu, *Adv. Funct. Mater.* **2016**, *26*, 2185.

[17] G. Yang, H. Gong, X. Qian, P. Tan, Z. Li, T. Liu, J. Liu, Y. Li, Z. Liu, *Nano Res.* **2015**, *8*, 751.

1702928 (10 of 10)